Biofouling, **33(9)** (2017) 703-711 doi:10.1080/08927014.2017.1359574

Measuring a critical stress for continuous prevention of marine biofouling accumulation with aeration

Mark Menesses[1], Jesse Belden[2], Natasha Dickenson[2], and James Bird[1]

[1]*Dept. of Mechanical Engineering, Boston University, Boston, Massachusetts, USA*
[2]*Naval Undersea Warfare Center, Division Newport, Newport, Rhode Island, USA*

Submitted 31 March 2017, Accepted 19 July 2017

Abstract

When cleaning the hull of a ship, significant shear stresses are needed to remove established biofouling organisms. Given that there exists a link between the amount of time that fouling accumulates and the stress required to remove it, it is not surprising that more frequent grooming requires less shear stress. Yet, it is unclear if there is a minimum stress needed to prevent macrofouling growth in the limit of continuous grooming. This manuscript shows that single bubble stream aeration provides continuous grooming and prevents biofouling accumulation in regions where the average wall stress exceeds approximately 0.01 Pa. This value is found by comparing observations of biofouling growth from field studies with complementary laboratory measurements that probe the associated flow fields. These results suggest that aeration and other continuous grooming systems must exceed a wall stress of 0.01 Pa to prevent macrofouling accumulation.

Keywords: Shear stress; grooming; bubble; aeration

Introduction

Estimates for the stress required to remove marine fouling organisms range from 1 Pa to 10^6 Pa[1–4]. These estimates are particularly relevant to seafaring vessels, as the extent of biofouling has implications for ship performance[5–7], economics[8,9], and biosecurity hazards[10]. Fouling associated with the smaller stresses can be removed using grooming techniques, such as wiping by divers. In contrast, fouling associated with larger stresses requires more intensive interventions, such as scraping, and may even require drydocking, as high removal stresses can also damage the hull coating.

An overview of biofouling colonization suggests a relationship between the range of stresses needed to remove fouling and the amount of time a submerged surface is exposed to the fouling environment (Figure 1). The establishment of a biofouling colony has traditionally been divided into progressive stages of surface conditioning, attachment, colonization, and growth[11]. Surface conditioning can occur over the first minutes to hour of wetting as organic substances accumulate on the submerged surfaces. These organics serve to condition the surface and provide settlement cues for certain microfouling species. The initial adhesion of early settling microorganisms is weak, and they often can be dislodged by a shear stress on the order of 1 Pa[3,4]. These microorganisms begin to replicate and secrete extracellular polymeric substances (EPS), resulting in a biofilm slime that displays a stronger adhesion strength and may facilitate the attachment of certain macrofouling species. Macrofouling larvae settle with initial adhesion strength on the order of 0.1 MPa[12]. After weeks to months of maturation, macrofouling adhesion can increase to greater than 1

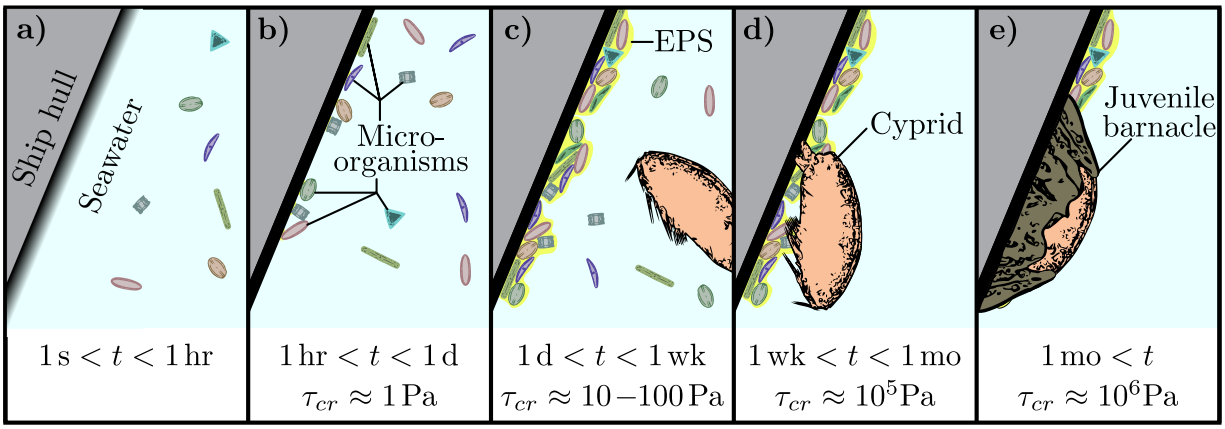

Figure 1: Illustration of fouling development noting the critical stress, τ_{cr}, for removal of fouling organisms with increasing immersion time, t. (a) Upon submersion, the fouling surface is conditioned as it collects organics present in the seawater. (b) After a short period of time, microorganisms begin to adhere to the conditioned surface. (c) Settled microorganisms secrete an extracellular polymer substance which encourages the growth of a surface biofilm. (d) Macrofouling larvae adhere to the surface. (e) Biofouling continues to grow as hardfouling (e.g. barnacle) matures. Note that illustration is not to scale.

MPa[1,2]. Contrary to traditional views of early biofouling succession, some algae and larvae can settle on clean surfaces in the absence of biofilms[13,14]. Indeed, the recruitment of macrofouling species has been extensively studied[15–19] and suggests that the succession in biofouling communities appears to be a dynamic process in which the species that ultimately settle depend on several factors, including substrate and biofilm characteristics, geographic location, season, and species interactions.

Regardless of the precise biofouling colonization dynamics, it appears that the time between grooming events governs the stress needed to clean a surface. Indeed, the relationship between stress and grooming frequency has been identified, with more frequent groomings needing lower stresses to remove fouling[20,21]. Extending this relationship to a limit, one might wonder: how low a stress is needed to keep the surface clean if the grooming technique were to operate continuously?

This manuscript seeks to find a minimum stress required to prevent biofouling accumulation as cleaning frequency increases to the limit of a continuous grooming scheme. In field experiments, test panels are submerged for several weeks as fouling develops. A distribution of continuous stresses is applied in the field tests using a stream of air bubbles, which is shown to prevent fouling growth in a local region. To gain insight into the velocities and stresses characteristic of the clean and fouled regions, flow measurements are recorded for locations within and adjacent to the bubble stream. By combining these laboratory measurements with the field results, a critical continuous stress value is identified above which the submerged surface remains free of macrofouling. This critical stress value is placed in the context of removal stresses required for intermittent cleaning reported in the literature.

Materials and methods

The inherent buoyancy of air bubbles was used to establish a continuous flow. This flow acted to move water and continually wipe the submerged surface. Fluid motion near a surface has long been known to influence biofouling growth[22–24], and aeration in the form of bubble curtains has been shown to prevent biofouling growth[25–28]. Rather than a curtain, a single stream of bubbles was used here to establish a narrow region of flow which inhibits biofouling growth locally.

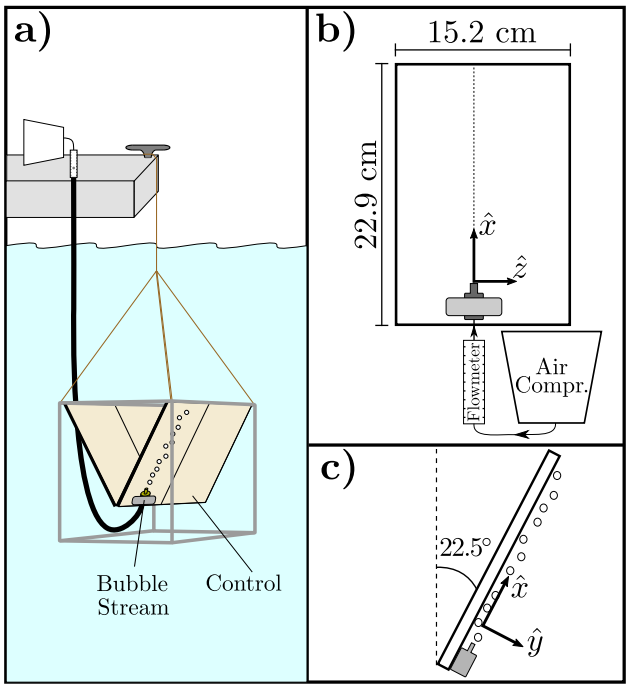

Figure 2: An illustration of the experimental rig setup: (a) A schematic representation of the field rig setup illustrating the orientation of the control and bubble stream panels. (b) Perpendicular view of test panel illustrating dimensions and axes. (c) Side view of test panel setup noting axes and tilt angle.Note that illustration is not to scale.

Flow setup

The test panel was submerged in water with a nozzle attached to the bottom, as shown in Figure 2. The flow was imposed along an underwater epoxy panel (garolite G-10) which was free of any coatings, had a smooth finish and was angled at 22.5° from vertical (Figure 2c). This angle was used previously in aeration experiments to mimic a ship hull[25]. The test panels had an elastic modulus of approximately 20 GPa[29] and were hydrophilic with a measured contact angle of 73.5°. These properties are not expected to inhibit the attachment and growth of marine fouling species.

The bubble stream was created with a nozzle 3.2 mm in diameter mounted at the bottom of the test panel and connected to an air compressor. In this flow, bubbles formed at the tip of the nozzle, pinched off, and rose along the inclined panel. The air flow rate was set to 150 mL/min using a needle valve. The bubble nozzle produced bubbles with a mean diameter of 5.2 mm with a standard deviation of 1.8 mm at an average rate of 24 bubbles per second.

Field experiments

Field experiments were carried out in Narragansett Bay, Rhode Island, USA, throughout the months of July and August in 2015, corresponding with the peak fouling season in the region. The average temperature in the bay during this period was approximately 21°C. The field rig consisted of a PVC framework onto which the test panels were attached: a control and bubble stream (Figure 2a). The rig was suspended off the side of a dock in a basin protected from local currents by a stone breakwater. The air flow rate was monitored consistently. The field rig was pulled from the water weekly, and photographs were taken of each test panel to record the fouling growth. The field experiments were concluded after seven weeks due to a constraint of test site availability.

Lab measurements

Each flow setup was duplicated in a large water tank to acquire particle image velocimetry (PIV) measurements in a laboratory setting. The tank was filled with tap water and seeded with 20-50 μm fluorescent tagged particles. The PIV setup consisted of a double pulsed Nd:YAG 532 nm laser (Litron NANO L 200-15) that was formed into a sheet in the $\hat{x}$-$\hat{y}$ plane (see Figure 2c). The laser light wavelength excited the seed particles, which re-emitted at a different wavelength (598 nm); this difference in wavelength allowed for optical filtering of the particle images such that reflections from bubbles were mitigated. The laser was synchronized to a digital camera (Lavision ImagerProX) that captured images in the frame-straddling PIV mode[30]. The camera was equipped with a 105 mm macro lens and gave a 27 mm x 27 mm field of view in the plane of interest.

PIV data were captured at multiple planes normal to the plate. Data sets of 5000 image pairs were captured for each plane. Image pairs were processed with two passes of 32 pixel x 32 pixel interrogation windows with 50% overlap. Velocity vectors were calculated from a cross-correlation of each interrogation window. Algorithmic masking was used for the bubble stream flow to prevent erroneous vectors caused by the distortion in the image due to the bubble presence as illustrated in Figure 3.

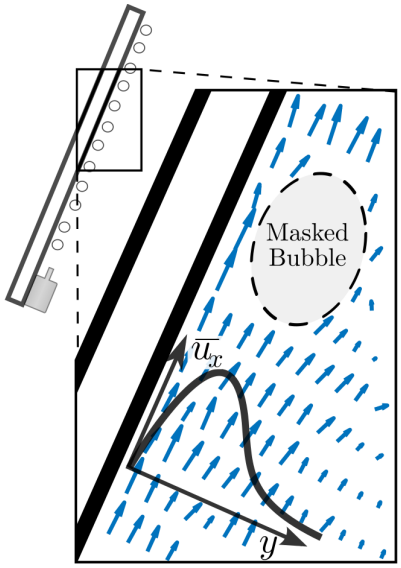

Figure 3: Illustration of data gathered from each PIV frame pair. The averaging process provided characteristic velocity curves with the tangential velocity, $\overline{u_x}$, versus the normal coordinate, y. Algorithmic masking was used to prevent erroneous vector calculation caused by passing bubbles.

Results

Field Results

Although significant fouling was evident on at least some regions of both panels, the bubble stream treatment contained a region with significantly less fouling over the course of the 7 week experiment, as shown in 4a. At this scale, the extent of microfouling was difficult to assess, and thus regions predominately unobstructed by fouling growth are henceforth referred to as 'clean'. The width of this clean region was larger than the bubble nozzle diameter on each respective panel and increased with distance from the nozzle. The extent of this region was marked by a sharp transition in the degree of fouling accumulation on the panel. To compare the percent coverage of macrofouling in the clean region to the control, a rectangular sample area was selected (box B and C in Figure 4a). Fouling type and coverage were assessed using random point image analysis

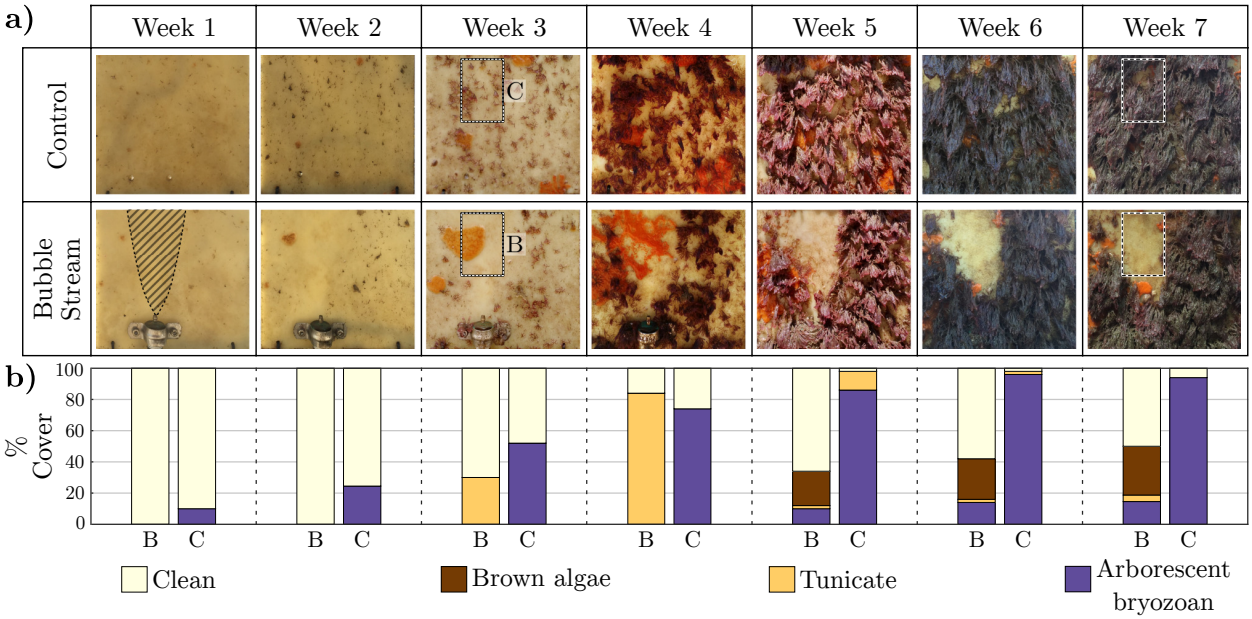

Figure 4: Progression of fouling growth throughout the duration of the experiment. (a) Images of the two test conditions, control (top row) and bubble stream (bottom row). The field tests were conducted during the summer of 2015 in Narragansett Bay, Rhode Island, USA. Images presented are cropped to better show the regions of flow. The crosshatched area in week 1 is a guide for the eye, representing the region in which flow was introduced. The boxes in week 3 images illustrate the areas used in the percent coverage. The rectangle area in week 3 identifies a region fully exposed to the bubble stream treatment, B, and the equivalent region on the control panel, C. (b) Percent of coverage of macrofouling species in region B and C. Organisms identifiable from macroscopic images were included in the percent coverage analysis. Any areas absent of identifiable macrofouling growth were noted as 'clean'.

software CPCe[31], which visually identified fouling organisms to the lowest possible taxonomic level. At the conclusion of the field campaign, the control sample area was nearly saturated with arborescent bryozoans (*Bugula sp.*); whereas, the bubble stream sample area was predominately clean (Figure 4b). The bubble stream sample area at week 7 consisted of 15% arborescent bryozoans, 4% colonial tunicates (*Botrylloides violaceus*), and 31% brown algae (*Phaeophyceae*), with the remainder visually unobstructed and therefore here referred to as clean. The percent coverage analysis also offers insight into the rate of growth in both the control and bubble stream sample areas. Fouling coverage of the control sample area increased at a rate of approximately 20% per week, whereas fouling coverage in the bubble stream area increased at a rate of approximately 7% per week. If these trends were to continue, brown algae might dominate the region within several months. Regardless, during the investigation period, the bubble stream treatment maintained a locally clean surface.

Away from the bubble stream, the fouling growth progressed similarly to the control sample area (Figure 4a). Close inspection of both panels revealed evidence of hard fouling consisting of juvenile barnacles (*Balanus sp.*), tubeworms (*Serpulidae*), and slipper snails (*Crepidula fornicata*); however, these organisms were too sparse to be identified by the detection algorithm and were eventually occluded by the dense coverage of arborescent bryozoans. One unexpected observation was the growth of a tunicate within the clean region during weeks 3-4 that receded by week 5 and was not evident thereafter.

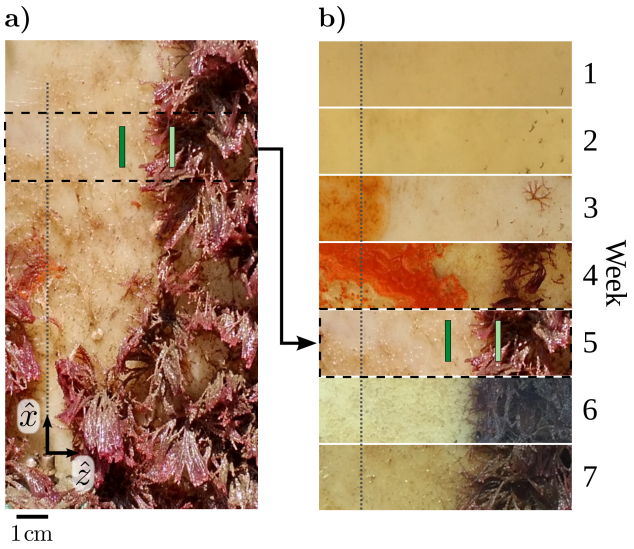

Figure 5: Illustration of the selection of the PIV plane locations. (a) A cropped portion of the bubble stream panel from week 5. The dark and light markers represent the clean and fouled regions investigated with PIV, respectively. (b) The evolution of fouling in this region of interest over the course of the field experiment.

Lab results

From the field results, representative clean and fouled regions were identified in the bubble stream flow, as shown in Figure 5. Each region was 1.30 cm long in the tangential direction centered at $x = 9.7$ cm. The clean and fouled regions were located at $z = 3.9$ cm and $z = 2.4$ cm, respectively. The clean regions selected indicated consistent lack of macrofouling growth with only microfouling present throughout the experiment while the fouled regions contained thorough macrofouling coverage. PIV measurements at each location provided velocity vectors on a Cartesian grid in the plane formed by axes normal and tangent to the test panels as illustrated in Figure 3. The velocities at each grid point were averaged over all samples providing a temporally averaged velocity field for each investigation region. Characteristic tangential velocity profiles were found by averaging the time-mean velocity fields along the tangential, or x, direction.

The water velocity in the clean region was faster than the water velocity in the fouled region (Figure 6). The value of the mean tangential velocity measurement nearest the wall in the clean region was $\overline{u_x}$ =3.7 cm/s. In the fouled region, the measurement nearest the wall was $\overline{u_x}$ =1.6 cm/s. Both velocity profiles trend to zero far from the wall. A velocity value of ~ 2.5 nearest the wall emerged as dividing the clean flow from the fouled flow. The standard deviation associated with each flow is shown by a shaded region in Figure 6. The size of these regions offers insight into the magnitude of fluctuations associated with each flow. On average, velocity fluctuations are on the order of the mean velocity for each flow.

Discussion

The bubble stream flow used in this experiment successfully achieved a reduction in biofouling settlement and growth. A swath of the test panel in high flow region showed greatly inhibited macrofouling growth. Additionally, the bubble stream flow used here shows the efficacy of a single stream of bubbles in local biofouling prevention in contrast to previous studies that relied on clouds of bubbles to achieve this effect[25–28].

As settling fouling organisms interact with the observed flow, they experience drag forces[32] which may provide a stress estimate. These drag forces are dependent upon the shape of the organism as well as its projected area normal to the direction of the flow. For an organism with an attachment area on the same order as its projected area and a Reynolds number much greater than one, the shear stress at the wall may

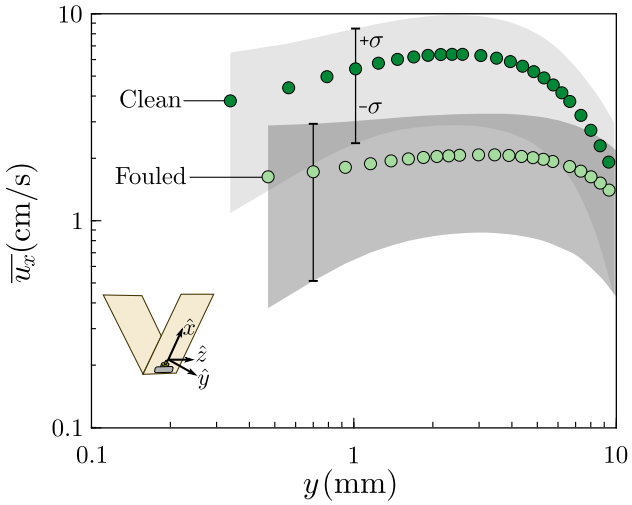

Figure 6: Mean tangential velocity, $\overline{u_x}$, versus normal coordinate, y, obtained from PIV measurements. Clean and fouled regions (corresponding to locations marked in Figure 5) are represented by the dark and light symbols, respectively. Shaded regions represent one standard deviation, $\pm\sigma$, for each flow

be related to the flow as $\tau_d \sim \rho u_x^2$ for a fluid with densith ρ and measured tangential velocity, u_x. An adhered arborescent bryozoan larva, whose size L range from 0.20-0.75 mm, would experience velocities similar to those collected nearest the wall, 1.6 cm/s and 3.8 cm/s for the fouled and clean regions, respectively. Thus the Reynolds number, $Re = \rho u_x L/\mu$ for a fluid with viscosity μ, in both locations is around 10, and the shear stress, τ_d, experienced by this larva settled between the fouled and clean regions would be between 0.2-1.2 Pa. It should be noted these values are considering the average velocity; however, for the standard deviation associated with these flows, the values of τ_d would be constrained to within an order of magnitude.

Different sized organisms would experience different stresses depending on the degree to which they extend into the velocity profile. Insight into the functional form of the velocity profile can be obtained by plotting it onto a semilogarithmic graph (Figure 7a). The data closest to the wall exhibits a logarithmic scaling. Indeed, such a scaling is expected in turbulent flows described by the canonical 'law of the wall' and can generally be expressed as

$$\overline{u_x} = \frac{u_\tau}{\kappa} \ln\left(\frac{y}{y_c}\right) \tag{1}$$

where y is the normal coordinate and κ is the von Kármán constant commonly accepted as 0.41. The length scale y_c is dependent upon individual flow characteristics such as eddy size and roughness while the friction velocity, u_τ, directly relates to the shear stresses at the wall, τ, as $u_\tau = \sqrt{\tau/\rho}$. In each velocity profile in Figure 7a, the logarithmic region is fit by the solid lines. Rewriting equation 1 as

$$\frac{\overline{u_x}\kappa\sqrt{\rho}}{\sqrt{\tau}} = \ln\left(\frac{y}{y_c}\right). \tag{2}$$

and using τ and y_c as fitting parameters, the logarithmic region of each flow collapses as shown in Figure 7b. The values of y_c found are 2.0 μm and 0.6 μm for the fouled and clean velocity profiles, respectively. The values of τ, which describe the shear stress at the wall, are 1.5 mPa and 40 mPa for the fouled and clean profiles, respectively. Plotting these stress values in Figure 7c illustrates a stress on the order of 10^{-2} Pa would be predicted between fouled and clean regions. An alternate way to estimate the shear stress is to note that for a distance close to the wall $\tau = \mu\frac{\Delta u_x}{\Delta y}$ where Δu_x takes the value of u_x at the distance Δy from the wall. Using the velocity points nearest to the wall for this estimate provides a value on the order of 10^{-4} Pa, which would be expected to be below the true shear stress given that the velocities used for this estimate are within the intertially governed logarithmic region of the velocity profile.

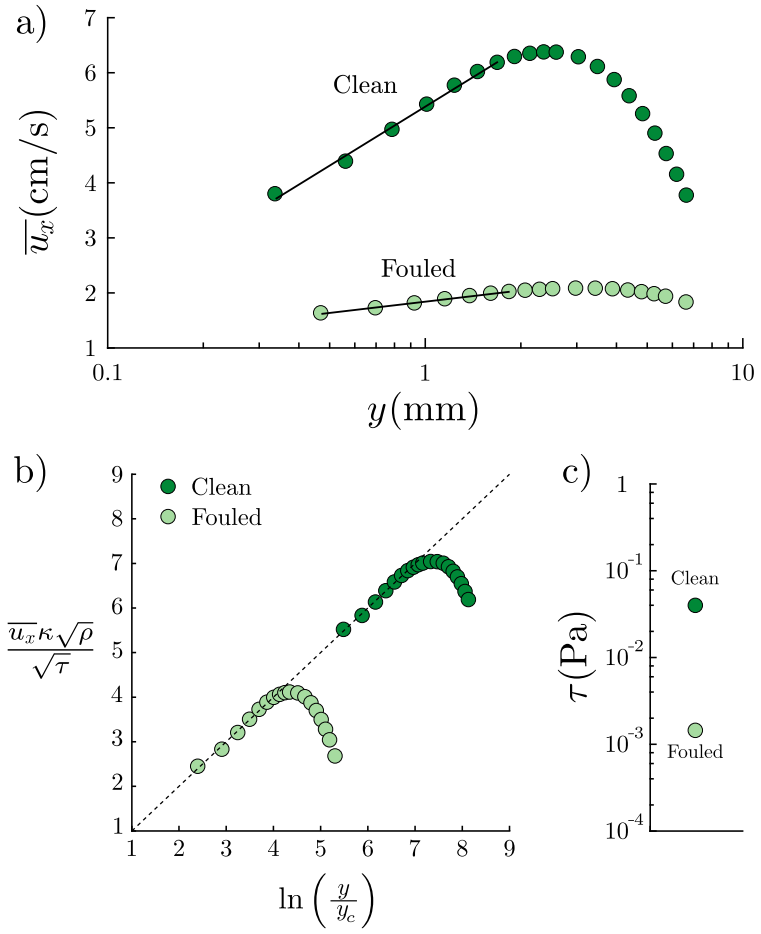

Figure 7: Analysis of velocity data with fitted stress values. (a) The characteristic velocity profiles for each flow rescaled on semilogarithmic plots. The line fits correspond to the law of the wall region for each velocity profile. (b) Nondimensionalized velocity profiles. Using adjustable parameters τ and y_c, all data for the logarithmic flow regions collapse to a line with a slope of 1 (dotted line). (c) Values of τ obtained from fitting velocity data to equation 2.

To place the stress values measured here in context, the critical stress values reported in literature for the removal of various fouling species are plotted versus immersion time in Figure 8. In general, for longer immersion times a fouling organism requires a higher critical stress for removal. For hard macrofouling organisms exposed to a substrate for over a year, critical stress required for removal can approach 1 MPa, whereas estimates of the adhesion strength for larvae adhered for one second are less than 1 Pa (Figure 8). In many of these studies, emphasis is placed the influence of substrate properties on the adhesion of fouling organisms. This variation in substrate is evident in the spread of critical stress values for a given organism and immersion time illustrated in Figure 8, where unprotected surfaces require larger shear than their fouling-release counterparts. The critical stress in the present study is measured on an unprotected epoxy substrate, and therefore might overestimate the critical stress required for continuous grooming on a surface with a fouling-release coating. However, because the distinction between lack of recruitment and fouling removal vanishes as a shear stress is continuously applied, the role of the substrate is less clear. Nevertheless, the wall shear stress estimated between the fouled and clean regions in the present study is significantly smaller than those needed to remove fouling organisms that reside on the surface a for a finite time.

The markedly smaller value of shear stress raises the possibility that other mechanisms of biofouling prevention via bubbles might be at play. In addition to the mechanism of fluid stress discussed herein, the presence of bubbles in the flow offers the opportunity for additional influence on the biofouling growth through direct interaction such as desiccation, scouring of the surface, or scavenging by capillary forces[33–35]. Additional field tests were performed using a water jet to induce flow along a test panel which found results in agreement with the bubble stream flow (see supplemental material). This agreement highlights that, in the regime of bubble stream flow tested here, the primary mechanism of influence on biofouling is the motion and stresses found in the liquid phase.

Water flow past a surface has long been known to reduce biofouling growth, and it has been suggested that flow velocities greater than 55 cm/s are necessary for prevention of biofouling accumulation[22]. Yet, in the present study, the measured velocities in the clean region are noticeably lower than 55 cm/s, a disparity evident in both the bubble stream and water jet flow experiments (Figure 6 and Figure S2). Fluid velocities generally decrease as they approach a stationary wall giving rise to a continuous velocity profile. Indeed,

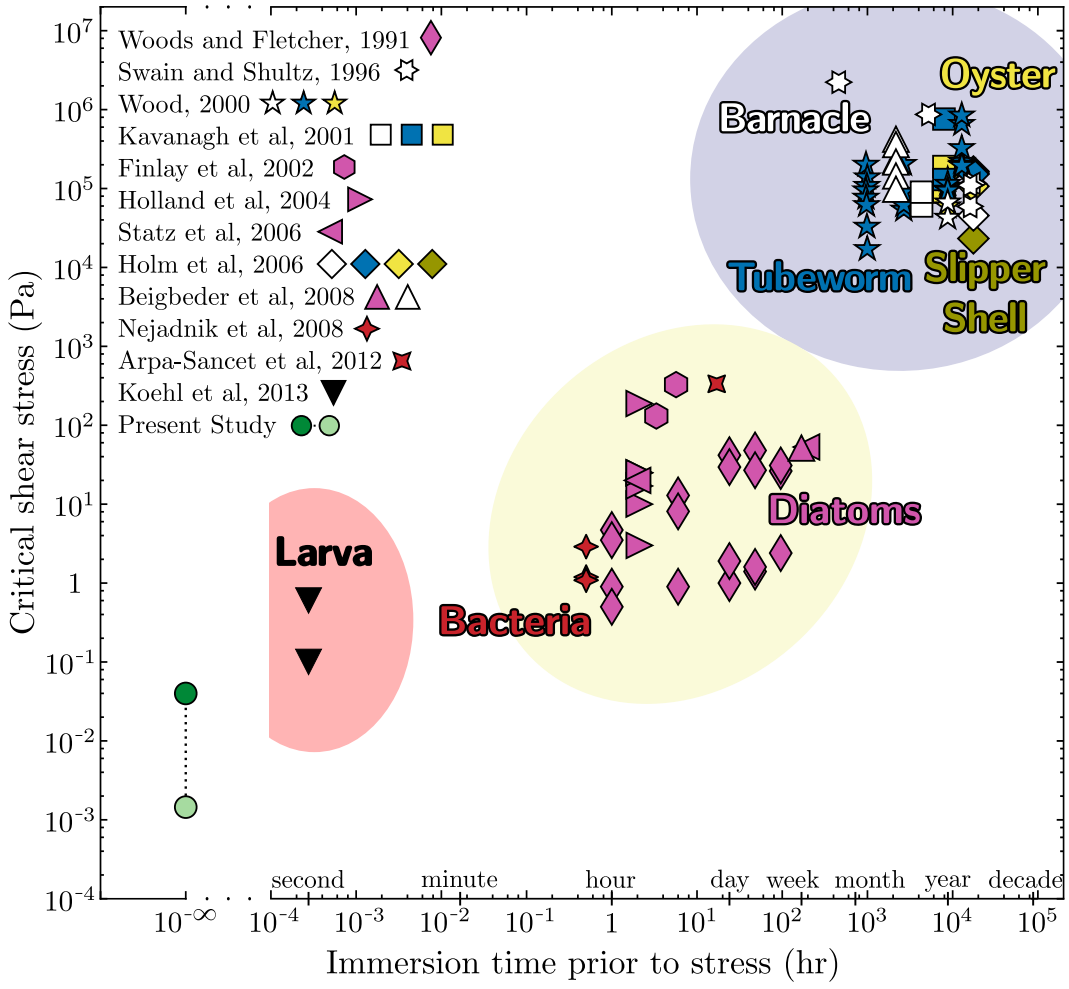

Figure 8: Critical stress values for removal of various biofouling organisms in the literature plotted versus immersion time prior to stress exposure. Stress values obtained from equation 2 are shown in addition to other values sourced from literature. Symbol shape denotes data source while symbol color denotes fouling type as described within the figure. Note, the break in the x-axis signifies the separation of continuously applied stresses (left) from stresses applied after discrete times (right).

without knowledge of this flow profile, it is challenging to estimate a shear stresses experienced by fouling organisms on the surface. Furthermore, the size of the fouling organism can influence the stress it experiences from the flow. Small organisms, such as bacteria and diatoms, may reside close enough to the surface to be protected by the viscous sublayer and experience shear stresses similar to the wall stress. By contrast, larger organisms, such as larval bryozoans and tunicates, extend into higher velocity flows such that larger stresses could lead to removal if adhered at the boundary between the clean and fouled region. In summary, through a combined field and laboratory study, the critical wall stresses necessary for prevention of biofouling growth using a continuous aeration scheme were found to be on the order of 10^{-2} Pa. These wall stresses are linked to the near-wall flow profile, which dictates the stresses felt by fouling organisms of various sizes. Indeed, the critical stress estimated earlier on an organism the size of an adhered bryozoan larva was approximately 1 Pa, which is similar to the theoretical stress necessary to remove a larva with an adherence time of 1 second (Figure 8). This critical stress value serves to further inform the development of grooming strategies. More specifically, this understanding of a critical continuous stress may assist in the optimization of aeration systems for the prevention of biofouling growth, should the stress field associated with rising bubble streams be understood.

Acknowledgements

The authors acknowledge C. Henoch and J.D. Hrubes for their assistance in PIV data collection, J. Rekos for his assistance with the field campaign, and E. Holm for helpful discussions.

Funding

This work was supported by the Office of Naval Research, Naval Undersea Research Program (grant no. N000141612171).

This material is based upon work supported by the National Science Foundation Graduate Research Fellowship Program under Grant No. DGE-1247312. Any opinions, findings, and conclusions or recommendations expressed in this material are those of the authors and do not necessarily reflect the views of the National Science Foundation.

References

1. Crisp, D., Walker, G., Young, G. & Yule, A. Adhesion and substrate choice in mussels and barnacles. *J Colloid Interface Sci* **104,** 40–50 (1985).
2. Swain, G. W. & Schultz, M. P. The testing and evaluation of non-toxic antifouling coatings. *Biofouling* **10,** 187–197 (1996).
3. Callow, M. E. & Callow, J. A. Marine biofouling: a sticky problem. *Biologist* **49,** 1–5 (2002).
4. Finlay, J. A., Callow, M. E., Ista, L. K., Lopez, G. P. & Callow, J. A. The influence of surface wettability on the adhesion strength of settled spores of the green alga Enteromorpha and the diatom Amphora. *Integr Comp Biol* **42,** 1116–1122 (2002).
5. Birnbaum, L., Bukzin, E. & Saroyan, J. Control of Ship Fouling in the US Navy. *Nav Eng J* **79,** 77–85 (1967).
6. Townsin, R. The ship hull fouling penalty. *Biofouling* **19,** 9–15 (2003).
7. Schultz, M. P. Effects of coating roughness and biofouling on ship resistance and powering. *Biofouling* **23,** 331–341 (2007).
8. Champ, M. A. A review of organotin regulatory strategies, pending actions, related costs and benefits. *Sci Total Environ* **258,** 21–71 (2000).
9. Schultz, M., Bendick, J., Holm, E. & Hertel, W. Economic impact of biofouling on a naval surface ship. *Biofouling* **27,** 87–98 (2011).
10. Molnar, J. L., Gamboa, R. L., Revenga, C. & Spalding, M. D. Assessing the global threat of invasive species to marine biodiversity. *Front Ecol Environ* **6,** 485–492 (2008).
11. Chambers, L. D., Stokes, K. R., Walsh, F. C. & Wood, R. J. Modern approaches to marine antifouling coatings. *Surf Coat Technol* **201,** 3642–3652 (2006).

12. Yule A. B.; Walker, G. The temporary adhesion of barnacle cyprids: effects of some differing surface characteristics. *J Mar Biol Assoc UK* **64** (02 May 1984).

13. Roberts, D., Rittschof, D., Holm, E. & Schmidt, A. Factors influencing initial larval settlement: temporal, spatial and surface molecular components. *Journal of Experimental Marine Biology and Ecology* **150,** 203–221 (1991).

14. Callow, M. E., Callow, J. A., Pickett-Heaps, J. D. & Wetherbee, R. Primary adhesion of Enteromorpha (Chlorophyta, Ulvales) propagules: quantitative settlement studies and video microscopy. *Journal of Phycology* **33,** 938–947 (1997).

15. Hadfield, M. G. & Paul, V. J. Natural chemical cues for settlement and metamorphosis of marine invertebrate larvae. *Marine chemical ecology,* 431–461 (2001).

16. Callow, J. A. & Callow, M. E. Trends in the development of environmentally friendly fouling-resistant marine coatings. *Nat Commun* **2,** 244 (2011).

17. Dobretsov, S., Abed, R. M. & Teplitski, M. Mini-review: Inhibition of biofouling by marine microorganisms. *Biofouling* **29,** 423–441 (2013).

18. Salta, M., Wharton, J. A., Blache, Y., Stokes, K. R. & Briand, J.-F. Marine biofilms on artificial surfaces: structure and dynamics. *Environmental microbiology* **15,** 2879–2893 (2013).

19. Sweat, L. H., Swain, G. W., Hunsucker, K. Z. & Johnson, K. B. Transported biofilms and their influence on subsequent macrofouling colonization. *Biofouling* **33,** 433–449 (2017).

20. Tribou, M. & Swain, G. The use of proactive in-water grooming to improve the performance of ship hull antifouling coatings. *Biofouling* **26,** 47–56 (2010).

21. Tribou, M. & Swain, G. Grooming using rotating brushes as a proactive method to control ship hull fouling. *Biofouling* **31,** 309–319 (2015).

22. Smith, F. W. Effect of water currents upon the attachment and growth of barnacles. *Bio Bull* **90,** 51–70 (1946).

23. Mullineaux, L. & Garland, E. Larval recruitment in response to manipulated field flows. *Mar Biol* **116,** 667–683 (1993).

24. Koehl, M., Crimaldi, J. & Dombroski, D. Wind chop and ship wakes determine hydrodynamic stresses on larvae settling on different microhabitats in fouling communities. *Mar Ecol Prog Ser* **479,** 47–62 (2013).

25. Scardino, A., Fletcher, L. & Lewis, J. A. Fouling control using air bubble curtains: protection for stationary vessels. *J Mar Eng Technol* **8,** 3–10 (2009).

26. Bullard, S. G., Shumway, S. E. & Davis, C. V. The use of aeration as a simple and environmentally sound means to prevent biofouling. *Biofouling* **26,** 587–593 (2010).

27. Dickenson, N. C., Warner, E. & Radicone, M. *Aeration methods for improved hull fouling prevention: using standard air and low dose elemental iodine infused bubbles for enhanced biolocigal interaction* tech. rep. (Naval Undersea Warfare Center Division, Newport, RI, Sept. 2014).

28. Dickenson, N. C., James, M. & Radicone, M. *Comparison of iodine infused aeration methods for biofouling prevention in temperate and tropical marine environments* tech. rep. (Naval Undersea Warfare Center Division, Newport, RI, Oct. 2015).

29. Ravi-Chandar, K. & Satapathy, S. *Mechanical properties of G-10 glass-epoxy composite* tech. rep. (TEXAS UNIV AT AUSTIN INST FOR ADVANCED TECHNOLOGY, 2007).

30. Raffel, M., Willert, C. E., Wereley, S. & Kompenhans, J. *Particle image velocimetry: a practical guide* (Springer, 2013).

31. Kohler, K. E. & Gill, S. M. Coral Point Count with Excel extensions (CPCe): A Visual Basic program for the determination of coral and substrate coverage using random point count methodology. *Computers & Geosciences* **32,** 1259–1269 (2006).

32. Koehl, M. Mini review: hydrodynamics of larval settlement into fouling communities. *Biofouling* **23,** 357–368 (2007).

33. Sharma, P. K., Gibcus, M. J., Van Der Mei, H. C. & Busscher, H. J. Microbubble-induced detachment of coadhering oral bacteria from salivary pellicles. *Eur J Oral Sci* **113,** 326–332 (2005).

34. Walls, P. L., Bird, J. C. & Bourouiba, L. Moving with Bubbles: A Review of the Interactions between Bubbles and the Microorganisms that Surround them. *Integrative and comparative biology,* icu100 (2014).

35. Khodaparast, S., Kim, M. K., Silpe, J. E. & Stone, H. A. Bubble-Driven Detachment of Bacteria from Confined Microgeometries. *Environmental Science & Technology* (2017).

Measuring a critical stress for continuous prevention of marine biofouling accumulation: supplemental material

Mark Menesses[a], Jesse Belden[b], Natasha Dickenson[b] and James Bird[a]

[a]*Department of Mechanical Engineering, Boston University, Boston, Massachusetts, USA*
[b]*Naval Undersea Warfare Center, Division Newport, Newport, Rhode Island, USA*

Dated: June 17, 2017

Effect of flow absent of bubbles on biofouling

This supplementary material reports additional experimentation originally conducted along side the primary reported experimentation.

Field experiments

Concurrent with the bubble stream field experiment, a water jet test panel was deployed to investigate the influence of fluid motion on biofouling growth without the presence of bubbles. The water jet system was comprised of a nozzle 6.4 mm in diameter mounted at the bottom of the test panel, similar to the bubble stream setup. This nozzle was connected to a water pump using PVC tubing which established a wall jet with the primary direction of flow upward and parallel to the panel surface. A secondary outlet from the water line allowed for the precise control of flow rate by diverting excess flow. The flow rate of the water jet was set to 1.25 L/min. Particle image velocimetry (PIV) measurements were recorded using a setup identical to that used for the bubble stream case.

Field results

Maximum fouling coverage of approximately 50% coverage was reached by week 7. Most of the fouling was concentrated in the lower two thirds of the panel and generally outside of the water jet stream path (shown in Figure S1). A V-shaped path starting from the nozzle was found to be clear of major fouling growth with a spreading angle of 17° from the nozzle center-line. The fouling community was composed primarily by soft fouling including biofilm slime, colonial tunicates, and arborescent bryozoans. Hard fouling was first observed at week 2 and initially consisted of juvenile barnacles. By week 7, the hard fouling community included barnacles, tubeworms, and slipper snails. Little to no fouling was present in the water jet stream path until week 5, where fouling was greatly reduced compared to the remainder of the panel. Also, a large

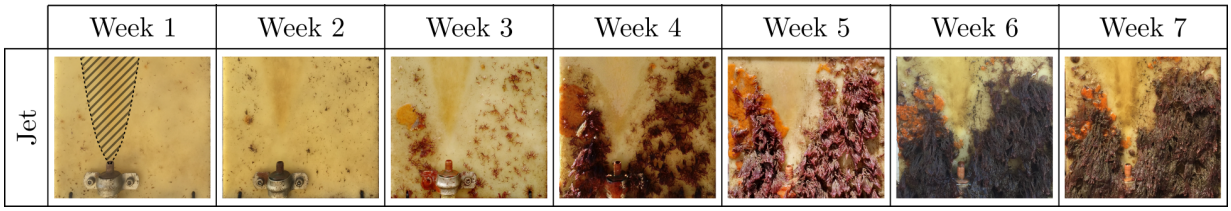

Figure S1. Progression of fouling growth throughout the duration of the experiment for water jet test panel. The field tests were conducted during the summer of 2015 in Narragansett Bay, Rhode Island, USA. Images presented are cropped to better show the regions of flow. The crosshatched area in week 1 is a guide for the eye, representing the region in which flow was introduced.

colonial tunicate mat which was present from weeks 3 through 5 in the top right corner of the panel had practically disappeared by week 6.

Lab results

Particle image velocimetry (PIV) was used to evaluate the flow characteristics at a representative clean and fouled region for the water jet. The clean and fouled regions were selected using the same criteria as described for the bubble stream (Figure S2-a). Characteristic velocity profiles were obtained using the averaging process described in the main text (Figure S2-b). From these velocity profiles, the water jet clean region showed a much higher average velocity, approximately 22 cm/s, than the corresponding fouled region, approximately 3.5 cm/s. Fitting these velocity profiles to the log-law relationship given in equation 2, the wall stress values for each region were obtained, as shown in Figure S2-c.

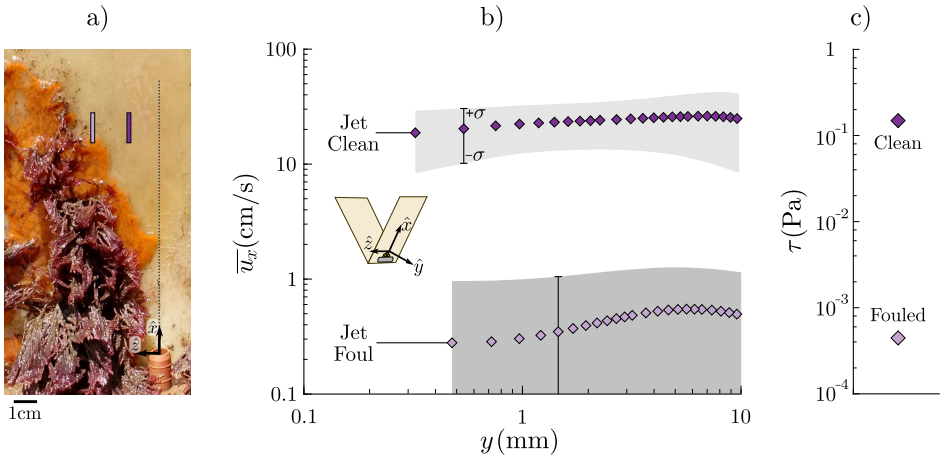

Figure S2. Results from PIV measurements and analysis for the water jet flow. (a) Representative clean and fouled regions were selected from the field results. (b) The characteristic velocity profiles for clean and fouled regions identified in the water jet field experiment. (c) Values of wall stress found for both the clean and fouled water jet locations.

Remarks

The stresses found in the water jet test are in agreement with those found from the bubble stream. The water jet values provide more separated bounding values and offered no additional insight into a minimum stress value necessary to reduce biofouling growth.